Structurally Transformable and Reconfigurable Hydrogel-Based Mechanical Metamaterials and Their Application in Biomedical Stents

Sirawit Pruksawan[1,], Rigel Lu Jun Teo[2], Yu Hong Cheang[3], Yi Ting Chong[1], Evelyn Ling Ling Ng[1], and FuKe Wang[1,*]*

[1]*Institute of Materials Research and Engineering (IMRE), Agency for Science, Technology and Research (A*STAR), 2 Fusionopolis Way, Innovis #08-03, Singapore 138634, Republic of Singapore*

[2]*College of Design and Engineering, National University of Singapore (NUS), 15 Kent Ridge Crescent, Singapore 117585, Republic of Singapore*

[3]*Nanyang Polytechnic; 180 Ang Mo Kio Avenue 8, Singapore 569830, Republic of Singapore*

* To whom correspondence should be addressed: sirawit_pruksawan@imre.a-star.edu.sg; wangf@imre.a-star.edu.sg

Abstract

Mechanical metamaterials exhibit several unusual mechanical properties, such as a negative Poisson's ratio, which impart additional capabilities to materials. Recently, hydrogels have emerged as exceptional candidates for fabricating mechanical metamaterials that offer enhanced functionality and expanded applications due to their unique responsive characteristics. However, the adaptability of these metamaterials remains constrained and underutilized, as they lack integration of the hydrogels' soft and responsive characteristics with

the metamaterial design. Here, we propose structurally transformable and reconfigurable hydrogel-based mechanical metamaterials through 3D printing of lattice structures composed of multi-shape-memory polyacrylic acid-chitosan hydrogels. By incorporating reversible shape-memory mechanisms that control the structural arrangements of the lattice, these metamaterials can exhibit transformable and reconfigurable mechanical characteristics under various environmental conditions, including auxetic behavior, with Poisson's ratios switchable from negative to zero or positive. These adaptable mechanical responses across different states arise from structural changes in lattice, surpassing the gradual changes observed in conventional stimuli-responsive materials. The application of these metamaterials in multi-mode biomedical stents demonstrates their adaptability in practical settings, allowing them to transition between expandable, non-expandable, and shrinkable states, with corresponding Poisson's ratios. By integrating multi-shape-memory soft materials with metamaterial design, we can significantly enhance their functionality, advancing the development of smart biomaterials.

Keywords: Hydrogel; Mechanical Metamaterial; Smart Material; Mechanical Property; Stent

1. Introduction

Mechanical metamaterials have recently attracted significant interest due to their extraordinary mechanical properties, such as a negative Poisson's ratio and negative thermal expansion, as opposed to the positive values seen in conventional materials, enabling functionalities that are not achievable with traditional materials[1-3]. Rather than relying on the inherent properties of the material, these mechanical metamaterials are fabricated using tailored structural designs through various engineering techniques, ranging from the macro to the nanoscale, to achieve unique mechanical behaviors[4, 5]. These properties are realized by employing various base materials—including metals[6], ceramics[7], polymers[8], and foams[9]—and show potential for possible applications across diverse fields, from electronic and wearable devices[10-12] to biomedical applications[13-15]. However, a major challenge currently limiting mechanical metamaterials is their lack of adaptability and versatility for real-world applications.

Hydrogels are exceptional candidates for enhancing the adaptability and versatility of mechanical metamaterials, owing to their unique responsive properties and softness, which distinguish them from other base materials[16-18]. The combination of hydrogel responsiveness and flexibility with the exceptional features of mechanical metamaterials offers new possibilities beyond those provided by other base materials[19]. Recent studies have increasingly explored hydrogel-based mechanical metamaterials, capitalizing on the responsiveness of hydrogels to various stimuli—such as pH[14], temperature[20], and light[21]— to enhance functionality along with their unique metamaterial characteristics. These metamaterials exhibit diverse mechanical features such as negative hydration expansion[22], auxetic behavior[13], geometric transformation[23], and programmable capabilities[24]. In particular, several studies have focused on developing hydrogel-based auxetic metamaterials characterized by a negative Poisson's ratio[13-15, 25, 26]. These hydrogels expand laterally when stretched, unlike conventional

materials, which contract. This unique mechanical response, driven by structural design rather than intrinsic material properties, enables the tuning of the mechanical behavior without altering the material constituents, thereby expanding the potential for designing advanced functional materials.

Although several smart hydrogel-based auxetic metamaterials have been developed[19], their responsiveness arises from the inherent properties of the hydrogels, while their mechanical metamaterial characteristics stem from structural design, with each function working independently. This lack of integration between the hydrogels' inherent characteristics and metamaterial design limits the potential to achieve synergistic performance and integrated functionality. As a result, current hydrogel-based auxetic metamaterials are limited to predefined mechanical characteristics and certain responsiveness, which restrict their adaptability and reconfigurability. While some research integrates metamaterial design with other shape-memory materials like polymers[27-31], their structural adaptability remains limited as compared to hydrogels. Hydrogels with their inherent softness and responsiveness, offer superior shape adaptability and offer greater design flexibility. This limitation restricts the potential of mechanical metamaterials and prevents the full integration of hydrogels' unique softness, responsiveness, and shape-memory capabilities within the content of mechanical metamaterials.

Through 3D printing of reversible multi-shape-memory hydrogels, we propose hydrogel-based metamaterials with mechanical transformability and reconfigurability. The shape-memory mechanisms within the polyacrylic acid-chitosan hydrogel system allow precise control over the material’s structural adaptation through reversible shape fixation and recovery in response to various environmental stimuli. These structural adaptations enable the metamaterial to modify its mechanical properties in response to stimuli based on a predefined design, unlike traditional hydrogel-based mechanical metamaterials, which are constrained by

limited structural adaptability and mechanical responsiveness. Our developed hydrogel-based metamaterials feature a transformable and reconfigurable lattice structure, with Poisson's ratios that can shift from negative, to zero, and then to positive depending on the applied stimulus. This proposed concept is further demonstrated through the fabrication of multi-mode stents for biomedical applications, which can transition among expandable, non-expandable, and shrinkable states, each exhibiting a distinct Poisson's ratio. By integrating the superior multi-shape-memory and softness characteristics of hydrogels with mechanical metamaterial design, this work significantly enhances the functionality and adaptability of metamaterials, paving the way for the development of advanced smart biomaterials in biomedical applications.

2. Experimental Section

2.1 Materials

Acrylic acid (99% purity) and N,N'-methylenebisacrylamide (MBAA), supplied by Sigma-Aldrich (Singapore), were used as the hydrogel monomer and crosslinker, respectively, and were used as received. The photoinitiator lithium phenyl-2,4,6-trimethylbenzoylphosphinate (LAP) was obtained from TCI Chemical (Singapore). Rhodamine B (95% purity) and low molecular weight chitosan were acquired from Sigma-Aldrich (Singapore) and used without further purification. Calcium chloride ($CaCl_2$), sodium hydroxide (NaOH), and hydrochloric acid (HCl) were purchased from Sigma-Aldrich (Singapore).

2.2 Preparation and 3D Printing of Hydrogels

Chitosan solution at 4% w/v was prepared by dissolving chitosan in a 2% w/v aqueous solution of acetic acid and stirring for 10 hours. Subsequently, the precursor for the polyacrylic acid-chitosan hydrogel was prepared as follows: Acrylic acid monomer, chitosan solution, and deionized (DI) water were mixed in a 40:40:60 weight ratio and sonicated for several hours to

ensure even dispersion of the components. MBAA crosslinker at 0.05% by weight and LAP photoinitiator at 0.5% by weight were then added to the dispersion and further sonicated. Rhodamine B was added at 0.05% by weight as a dye to enhance visualization and printing accuracy. The resulting precursor was continuously stirred to ensure even dispersion and stored in a dark environment until further use.

The hydrogel precursors were 3D printed using an Anycubic Photon Mono 4K printer with a liquid crystal display (LCD) shadow masking technique (Anycubic Technology Co., Ltd., Shenzhen, China). The 3D models were created in stereolithography (STL) format using AutoCAD (Autodesk, Inc., San Rafael, CA, USA) and imported into Anycubic Photon Workshop for slicing. The lattice structure with a negative Poisson's ratio was 3D printed from the prepared hydrogel precursor, serving as the original shape sample. The stent specimen, featuring a negative Poisson's ratio structure, was initially 3D printed in sheet form and then rolled up to form a hollow cylindrical structure. The edges were sealed with the same hydrogel precursor to complete the stent. The thickness of each printing layer was set to 0.05 mm, with a light intensity of 70% and an exposure time of 30 seconds per layer. After importing the slicing file, the prepared hydrogel precursor was poured into the printer's vat, and the printing proceeded layer by layer. After printing, the hydrogel samples underwent post-curing in a UV oven and were soaked in DI water until they reached equilibrium, before being stored in a refrigerator for further testing or characterization.

2.3 Shape Memory Characterization

The shape fixity and recovery ratios were evaluated for hydrogel strip specimens to characterize their shape memory properties. The hydrogel strips were bent at a 180-degree angle to establish a temporary shape, which was held in either $CaCl_2$ or NaOH for a specified duration. Afterward, the applied bending force was released, and the shape fixity ratio was

assessed using the angle held during this fixation as the *deformed angle* and the angle of the hydrogel strip after bending as the *temporary fixed angle*. The hydrogel strips were then released from their temporary shape by soaking in DI water (for the $CaCl_2$-soaked strips) or HCl (for the NaOH-soaked strips) for a designated period. The shape recovery ratio was then evaluated. The angle of the hydrogel strip after the recovery process is referred to as the *final angle*. The hydrogel strips could be further soaked in the respective solution to determine a second round of shape fixity and shape recovery ratios. The following equations present the formulations for calculating the shape fixity and shape recovery ratios:

$$Shape\ fixity\ ratio\ = \frac{\theta_{Temporary\ fixed\ angle}}{\theta_{Deformed\ angle}} \times 100\% \quad \text{(Equation 1)}$$

$$Shape\ recovery\ ratio\ = \frac{\theta_{Deformed\ angle} - \theta_{Final\ angle}}{\theta_{Deformed\ angle}} \times 100\% \quad \text{(Equation 2)}$$

The shape memory of lattice structures was further characterized using a similar method to tune the auxeticity of the structure, which primarily consists of three main types: (1) Auxetic lattice structure (negative Poisson's ratio), (2) Zero Poisson's ratio lattice structure, and (3) Non-auxetic lattice structure (positive Poisson's ratio), as outlined in Figure S1 of the Supporting Information. The original lattice structure was shape-fixed in a designed mold using either saturated $CaCl_2$ or NaOH until equilibrium was achieved, thus obtaining a temporary shape (Figure S2 of the Supporting Information). The shape was then recovered in either DI water or HCl till equilibrium. Additionally, a multi-stage shape memory process was performed by utilizing different concentrations of $CaCl_2$ solution to fix different shapes in sequence and recover those shapes in DI water.

2.4 Morphological, Mechanical, and Physicochemical Characterizations

Field-emission scanning electron microscopy (SEM) was utilized to analyze the morphology of the polyacrylic acid-chitosan hydrogel in various states. Rectangular hydrogel samples,

approximately 1.5 cm × 1.5 cm × 1.5 cm in size, were prepared using a JEOL JSM6700F electron microscope (JEOL Co., Japan) operating at 5 kV. After an overnight freeze-drying process, the specimens were fractured in liquid nitrogen and mounted onto aluminum stubs with conductive carbon tape to observe their cross-sectional surfaces. A sputter-coating process was then performed using a JEOL JFC-1600 auto fine coater (Japan) to deposit gold for 40 seconds.

Tensile testing of hydrogels in various states was carried out using an Instron 5569 dual-column universal testing machine (Instron Co., USA) with a 100-N load cell, following ASTM D638 guidelines, in a manner similar to our previous measurements[32]. Hydrogel samples, cut into strips, were secured using pneumatic grips. The samples were stretched at a rate of 40 mm/min until they fractured. To ensure accuracy, at least three specimens were tested for each condition, with the results averaged and presented with standard deviation. The tensile strength was determined by dividing the maximum load by the specimen's original cross-sectional area. The tensile modulus was calculated from the initial linear portion of the tensile stress-strain curve.

Swelling tests of hydrogels in different solutions at equilibrium were conducted at room temperature. The hydrogel samples were prepared as square strips with approximate dimensions of 1.5 × 1.5 × 0.2 cm and were oven-dried overnight. The specimens were then initially weighed before immersing in their respective solutions for 24 hours. After soaking, they were removed, gently wiped to eliminate surface moisture, and weighed to determine their equilibrium weight. The equilibrium swelling ratio for each solution (DI water, saturated $CaCl_2$, and saturated NaOH) was calculated as the percentage increase in weight from the initial weight (W_i) to the equilibrium weight (W_e) using the following formula:

$$Swelling\ ratio = \frac{W_e - W_i}{W_i} \times 100\% \qquad \text{(Equation 3)}$$

The Poisson's ratio of hydrogels in lattice form across different states was measured using a 300 dpi resolution video camera, following a similar method as our previous report[13]. The hydrogel lattice structures were secured at both ends with wires and clamped using a universal testing machine (Instron Co., USA). Two points were marked on the specimen's surface in both the lateral and longitudinal directions. Movements of these points during tensile testing at a strain rate of 10 mm/min were tracked and recorded using Image J software (National Institutes of Health, USA). The lateral and longitudinal strains were then calculated, and the Poisson's ratio was determined by dividing the negative lateral strain by the longitudinal strain (Equation 4). The Poisson's ratio was measured for each unit in the lattice structures, and the average values were reported. For hydrogel stent specimens, the diameter change ratio (DCR) was calculated as the percentage increase in diameter from the original (D_i) to a specified point (D_t) at the stent's center (Equation 5).

$$Poisson's\ ratio\ = -\frac{Lateral\ strain}{Longitudinal\ strain} \quad \text{(Equation 4)}$$

$$Diameter\ change\ ratio\ = \frac{D_t - D_i}{D_i} \times 100\% \quad \text{(Equation 5)}$$

2.5 Finite Element Analysis Simulation

The finite element analysis (FEA) was performed using AutoCAD Inventor (Autodesk, USA) to simulate static stress under various strain conditions. This allowed us to observe structural changes and calculate the corresponding Poisson's ratios for comparison with experimental results. Different material properties, as outlined in Table S1 of the Supporting Information, were input into the simulation, and the material size was adjusted to match the experimental specimen. After defining the materials, a fixed constraint was applied to the structure, followed by a normal force to replicate the conditions of the experimental mechanical tests, achieving the target tensile strain levels. The Poisson's ratio of each lattice structure at specific strain

levels was calculated using the same method described earlier, by marking points on the surface of the specimen model. For the stent models (Figure S3 in the Supporting Information), the same simulation protocol was applied, and the DCR was calculated based on the simulated model accordingly.

3. Results and Discussion

3.1 Design of Mechanical Transformable and Reconfigurable Hydrogel Lattice Structure

A reversible multi-shape memory hydrogel capable of transitioning among three distinct shapes in response to different environmental stimuli was developed using a multinetwork polyacrylic acid/chitosan system (Figure 1). Composed of polyacrylic acid (PAA) and chitosan, this hydrogel serves as a model for reversible multi-shape memory systems. It can transition between multiple pre-defined shapes in response to external stimuli and revert without permanent deformation. This unique property enables the precise formation and reversal of various structural configurations, owing to its high shape fixity, recovery, reversibility, and responsiveness, defining the material's mechanical response. The primary network, composed of PAA, establishes the hydrogel's original shape in deionized (DI) water, providing structural integrity. The secondary network forms through chitosan chain entanglements in saturated saline solutions like $CaCl_2$, as chitosan chains self-assemble[33, 34]. This enables the hydrogel to maintain a temporary shape in saturated saline solutions and revert to its original shape when it is diluted with DI water. The tertiary network forms through the microcrystallization of chitosan in NaOH solution, driven by the deprotonation of chitosan's amine groups under alkaline conditions[35, 36]. This allows the hydrogel to hold a second temporary shape in an alkaline solution and revert to its original form when placed in an acidic solution. This multi-shape memory system facilitates the fabrication of mechanically transformable and

reconfigurable hydrogel lattice structures that can adopt three distinct configurations: (1) *Original Shape* in DI water, (2) *Temporary Shape I* in saline solution, and (3) *Temporary Shape II* in alkaline solution. The responsiveness of hydrogel systems based on these stimuli can be tuned within a desired range to suit practical applications for activating or deactivating the multi-shape memory process. To achieve responsiveness under other stimuli such as temperature or light, alternative reversible multi-shape memory hydrogel systems can be employed. However, their suitability and mechanical performance depend on factors such as shape fixity, recovery, and responsiveness, which can vary across different systems.

Using the developed hydrogel, three different lattice structures were designed to switch between one another, exhibiting varying Poisson's ratio characteristics ranging from negative to zero to positive (Figure 1 and Figure S1 of the Supporting Information). The negative Poisson's ratio corresponds to a re-entrant hexagonal honeycomb lattice structure, while the positive Poisson's ratio is achieved with a standard hexagonal honeycomb lattice[13]. On the other hand, the zero Poisson's ratio is realized through a half re-entrant honeycomb lattice structure[37]. The negative Poisson's ratio structure regarded as *Original Shape* in DI water, which can be reshaped into a positive Poisson's ratio structure, referred to as *Temporary Shape I*, upon immersion in $CaCl_2$, and subsequently revert to its original shape when returned to DI water. Similarly, it can transition into a zero Poisson's ratio structure, designated as *Temporary Shape II*, in NaOH and revert to its original shape in HCl. This highlights the adaptability and versatility of the reversible multi-shape memory hydrogel system as a soft metamaterial, capable of altering its shape in various forms while demonstrating effective shape memory behavior across diverse environments.

The switching among the three lattice structures enables the transformation of their Poisson's ratio, or auxeticity, into three different modes of expansion when stretched: (1) non-expandable, (2) expandable, and (3) shrinkable, as illustrated in Figure 1. The positive

Poisson's ratio structure represents conventional materials, which typically contract laterally when stretched longitudinally, corresponding to the shrinkable mode. The negative Poisson's ratio represents a special case where the material expands laterally when stretched longitudinally, corresponding to the expandable mode[13, 38, 39]. The zero Poisson's ratio indicates that the material exhibits no change or minimal change in lateral dimensions when stretched, corresponding to the non-expandable mode[40]. These three modes of expansion encompass all possible auxetic responses and can be utilized in various applications focusing on mechanical response, such as biomedical stents[41, 42], where different expansion modes are required in varying environments. To demonstrate their application, multi-mode biomedical stents capable of transitioning among non-expandable, expandable, and shrinkable modes were fabricated according to the 3D model designs shown in Figure S3 of the Supporting Information and subjected to stretching tests. The following sections detail the shape memory and mechanical behavior of the reversible multi-shape memory hydrogel (Sections 3.2 and 3.3), the fabrication and configurability of its transitional lattice structures (Sections 3.4 and 3.5), and their applications for multi-mode biomedical stents (Section 3.6).

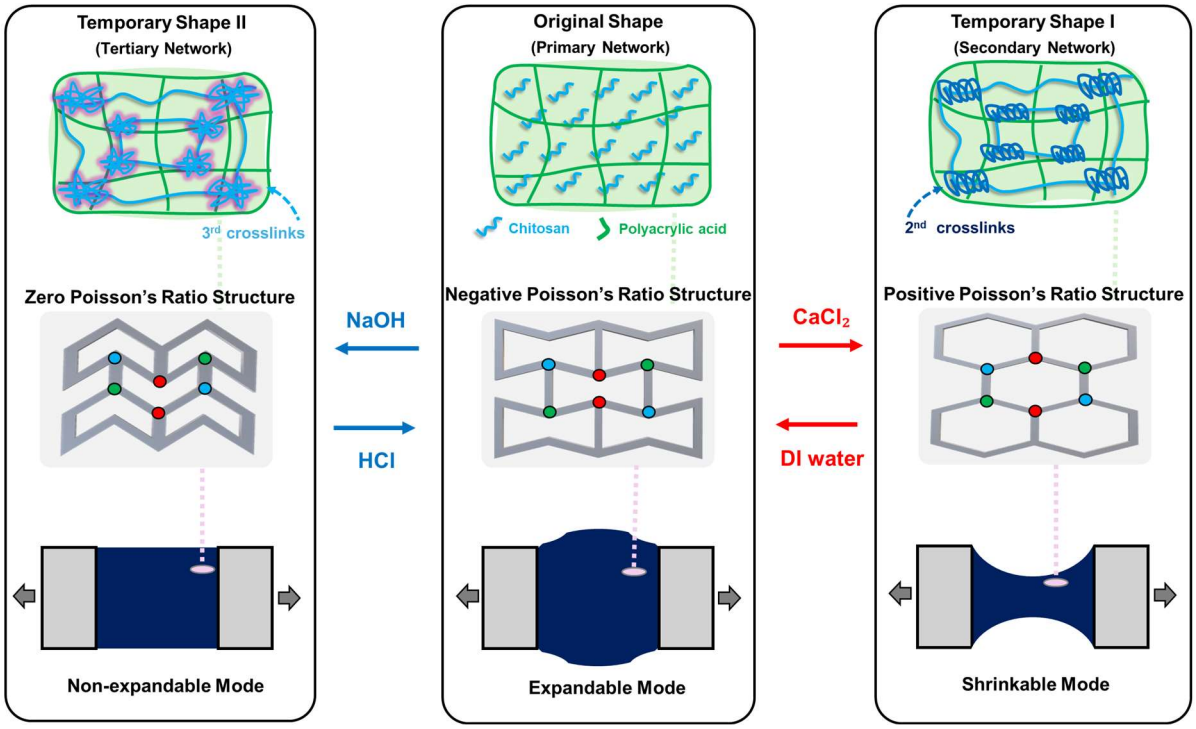

Figure 1. Hydrogel-based metamaterials with mechanical transformability and reconfigurability based on multi-network shape memory hydrogel and its application in multi-mode biomedical stents.

3.2 Shape Memory Behavior of Polyacrylic Acid/Chitosan Hydrogels

The shape memory behavior of the PAA/chitosan hydrogels is characterized, as shown in Figure 2. As discussed in previous sections, two mechanisms for shape retention are utilized: (1) chitosan chain entanglements in saturated $CaCl_2$ solution and (2) chitosan microcrystallization in saturated NaOH solution. As illustrated in Figure 2a, a strip specimen is fixed into a temporary shape with a 180-degree bend in either $CaCl_2$ or NaOH solutions, and the shape fixity ratio is evaluated over soaking time. In saturated $CaCl_2$ solution, the shape fixity ratio shows a sharp increase between 15 and 20 minutes, achieving 97.3% at 25 minutes. In contrast, in saturated NaOH solution, the shape fixity ratio increases rapidly, exceeding 90% within just 5 minutes and reaching 99.7% at 25 minutes. This suggests that shape fixing in

saturated NaOH occurs more rapidly than in $CaCl_2$, likely due to the low molecular weight of chitosan in this work, which has a limited chain length but high chain mobility[43]. This would facilitate the formation of ordered crystalline structures in the alkaline solution more rapidly than chain entanglements formation in the saline solution. In both cases, an almost complete shape fixity ratio is achieved within 25 minutes, demonstrating notable shape memory characteristics[44]. Due to the reversible physical interactions between chitosan and the polymer network, the shape-fixed hydrogel can be reverted to its original form and reshaped into new temporary shapes, either in the same solution or a different one. Figure 2b further illustrates the effect of $CaCl_2$ and NaOH concentration on shape fixity ratios, showing that equilibrium shape fixity capability increases with solution concentration. Shape memory capacity approaching 100% at equilibrium can be achieved with concentrations close to saturation.

To recover the $CaCl_2$-fixed specimen to its original shape, DI water was used to dilute the saline solution, dissociating the self-assembly of chitosan. Upon soaking in DI water, the strip specimens gradually returned to their original shape, achieving a shape recovery ratio of 99.7% within 15 minutes (Figure 2c). For the NaOH-fixed specimens, recovery is facilitated by an acidic solution of 0.1 M HCl, resulting in a rapid recovery of 96.7% within just 2.5 minutes, indicating prompt dissolution of chitosan microcrystallization, even at this low concentration. The reversibility of shape fixing and recovery is evaluated by repeatedly soaking the strip specimens in their respective solutions for 25 minutes, as shown in Figure 2d. It was observed that, in saturated $CaCl_2$ solution, the equilibrium shape fixity ratio slightly decreased by 4.1% in the second cycle and by 3.2% in the third cycle compared to the equilibrium shape fixity in the first cycle. In saturated NaOH solution, the reduction in equilibrium shape fixity was more pronounced, with decreases of 16.1% in the second cycle and 22.8% in the third cycle. This suggests a higher reversibility of the ionic bonds between calcium ions (Ca^{2+}) and the negatively charged groups on the chitosan network, facilitating the entanglement and

disentanglement of chitosan chains in $CaCl_2$ solution[33]. In contrast, repeated deprotonation and recrystallization of chitosan in NaOH exhibit lower reversibility due to their greater impact on the hydrogel's integrity. The results confirm the reversible multi-shape memory system of the PAA/chitosan composite developed in this work, demonstrating high shape fixity and recovery ratios through the standardized strip bending test, which enables comparison with other materials. This will further illustrate the shape memory performance of more complex structures, such as lattice structures or stents, enabling mechanical responses in different shapes.

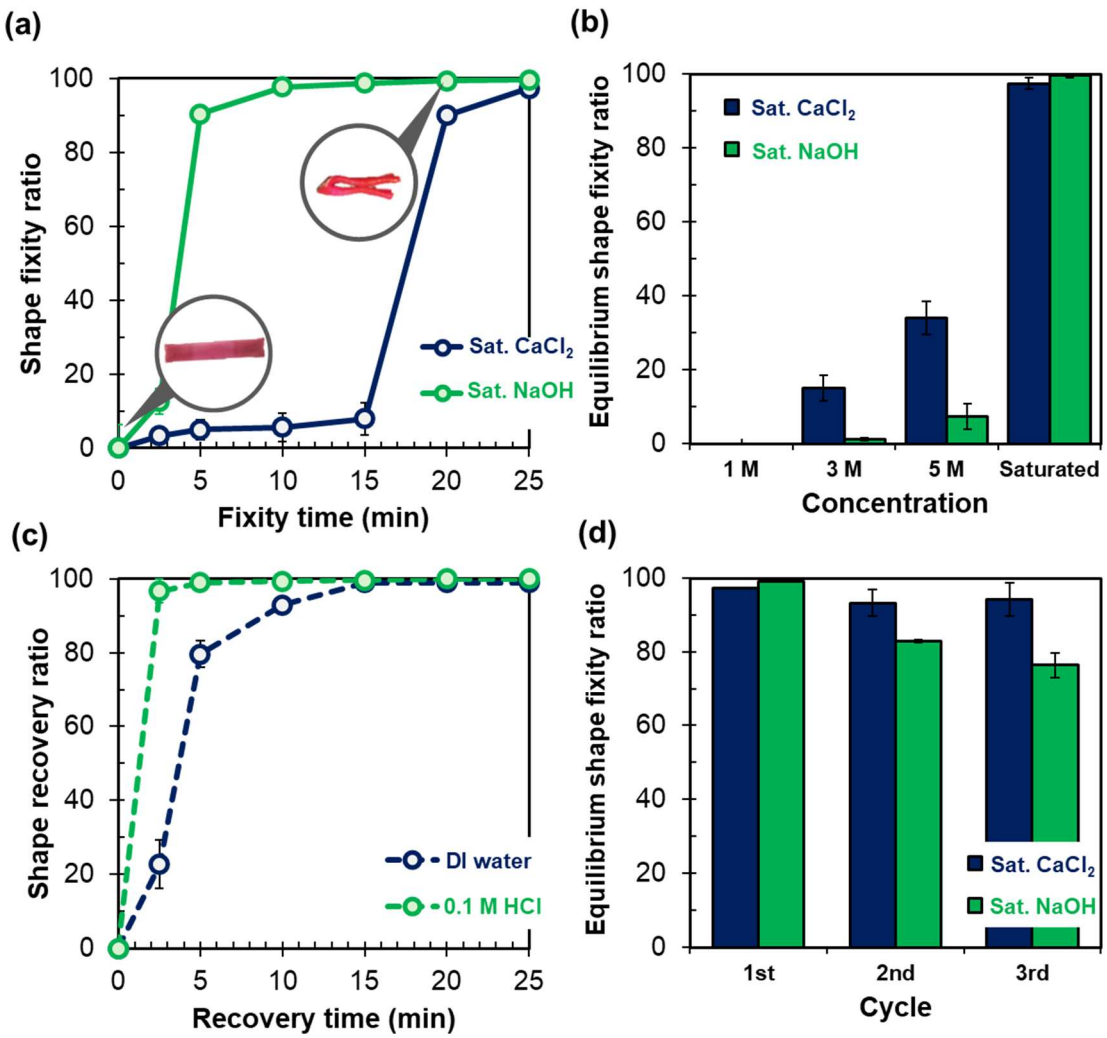

Figure 2. Multi-shape memory properties of polyacrylic acid/chitosan hydrogels. (a) Shape fixity ratios of the hydrogels as a function of fixity time in saturated $CaCl_2$ and NaOH solutions. (b) Equilibrium shape fixity ratios of the hydrogels in varying concentrations of $CaCl_2$ and NaOH solutions. (c) Shape recovery ratios of the hydrogels as a function of recovery time in H_2O and 0.1 M HCl solutions. (d) Equilibrium shape fixity ratios of the hydrogels in saturated $CaCl_2$ and NaOH solutions across the first three fixing cycles.

3.3 Morphological, Mechanical, and Physicochemical Properties of Polyacrylic Acid/Chitosan Hydrogels

The multi-shape memory behavior of PAA/chitosan hydrogels is elucidated through detailed morphological, mechanical, and swelling characterizations across varied states (Figure 3). In DI water, the hydrogel exhibits a typical macroporous structure due to the crosslinked PAA network, which retains water and forms substantial pores within the material (Figure 3a, left). Upon immersion in saturated $CaCl_2$ solution until equilibrium, the hydrogel's microstructure becomes noticeably denser (Figure 3a, center), with a reduction in both pore size and pore number, indicating the formation of an additional chitosan network through chain entanglements. This dense network helps stabilize the deformed shape, preventing the material from returning to its original configuration. The deformed shape can be reverted to its original form by dissolving the entanglements upon dilution with DI water. Similarly, immersion in saturated NaOH solution results in a dense network morphology that stabilizes another deformed shape (Figure 3a, right), but through the formation of chitosan microcrystallization. This densification in microstructure corresponds with the mechanical properties shown in Figure 3b, where both tensile strength and strain at break are significantly enhanced after soaking in saturated $CaCl_2$ and NaOH solutions.

The hydrogel soaked in $CaCl_2$ demonstrates an exceptionally high tensile strength of 4.3 MPa and a strain at break of 1,231%, confirming the formation of a robust chitosan-entangled network induced by Ca^{2+} (Figure 3b and Table S2 of the Supporting Information). This hydrogel exhibits an average toughness of 20 MJ/m^3, significantly surpassing many reported toughened hydrogels, such as hydrogel composites[32, 45-47] and double-network hydrogels[48, 49]. Furthermore, the hydrogel exhibits "extreme mechanical metamaterial" characteristics, enabling highly tunable mechanical properties that range from soft to extremely tough[19, 50]. Specifically, the tensile strength can be increased from an initial 0.05 MPa to 4.3 MPa, representing an 860-fold enhancement. The NaOH-treated hydrogel also shows notable improvements in mechanical properties compared to its original state, achieving a tensile strength of 0.5 MPa and a strain at break of 633%. However, these enhancements remain less pronounced than those attained through $CaCl_2$ treatment. This likely arises from $CaCl_2$ facilitating additional ionic crosslinking between PAA and chitosan chains, while NaOH primarily promotes the formation of the chitosan network through its own microcrystalline domains. Notably, this work utilizes low molecular weight chitosan, which may enhance chain mobility and flexibility[51], potentially enabling better energy dissipation and improved interfacial interactions compared to the higher molecular weight chitosan used in previous studies[33, 35].

To further elucidate its physicochemical properties, the swelling behavior of the hydrogel at equilibrium in various states is shown in Figure 3c. The hydrogel exhibits a significant swelling capacity in DI water compared to its dried state, with a swelling ratio of up to 607%. In contrast, soaking the hydrogel in saturated $CaCl_2$ solution results in a significantly lower swelling ratio of 8%. This reduced swelling is due to the considerably denser microstructure formed by Ca^{2+}, as discussed previously. When soaked in saturated NaOH, the hydrogel displays a reduced swelling ratio of 278%, indicating the formation of a

moderately dense microstructure due to chitosan crystallization. These results clearly demonstrate the hydrogel's responsiveness to different solutions at the microstructural level, attributed to the formation and removal of the additional chitosan network, resulting in a highly adaptive shape memory hydrogel system.

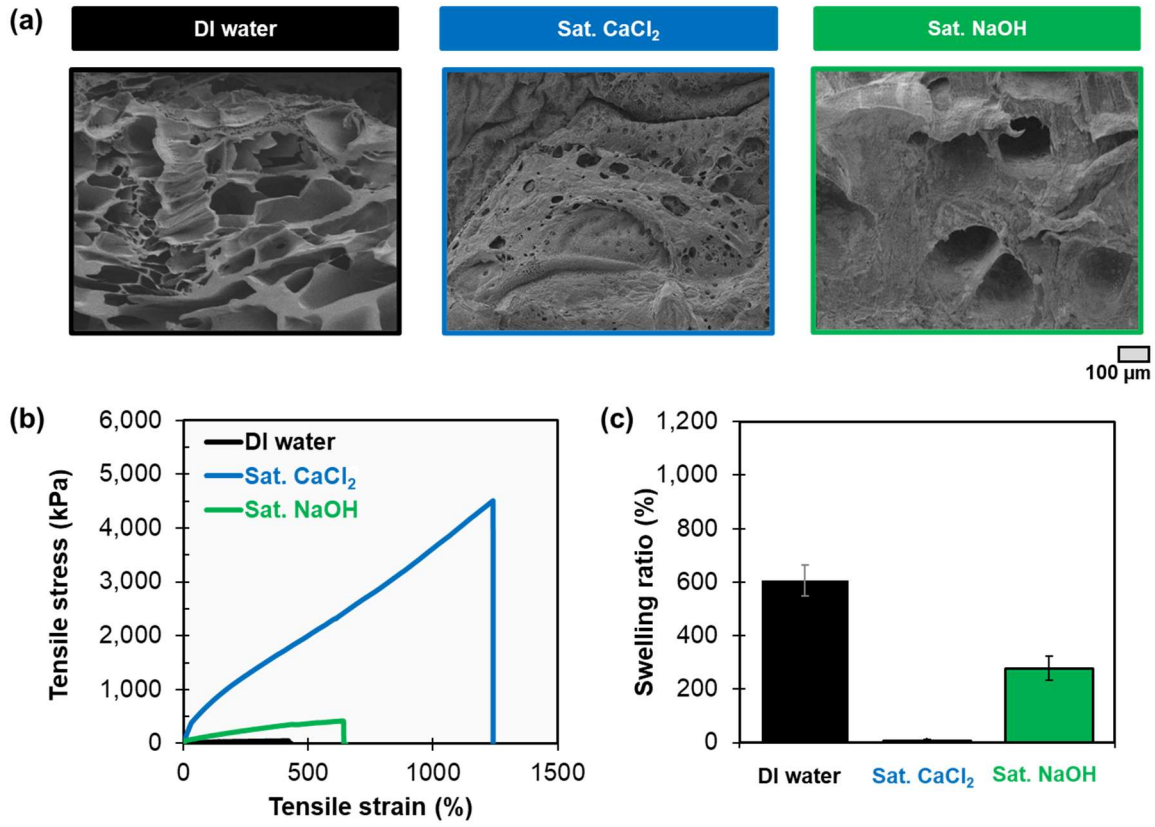

Figure 3. Morphological, mechanical, and physicochemical properties of polyacrylic acid/chitosan hydrogels. (a) Scanning electron microscope (SEM) images, (b) tensile stress-strain curves, and (c) equilibrium swelling ratios of hydrogels soaked in water, $CaCl_2$, and NaOH solutions. The tensile stress-strain data from a single specimen is presented as a representative curve, while the full average values with standard deviations are provided in Table S2 of the Supporting Information.

3.4 Multi-shape Memory Behavior and Corresponding Mechanical Properties of Hydrogel Lattice Structures

The multi-shape memory hydrogel is employed to fabricate transformable and reconfigurable lattice structures through 3D printing. These printed lattice structures were shape-fixed in a mold using either saturated $CaCl_2$ or NaOH solutions to achieve specific structural configurations, allowing the lattice structure to adapt its shape in response to external stimuli. The protocol for fixing the lattice structure into different shapes within a mold is provided in Section 2.3 and Figure S2 of the Supporting Information. Figure 4a illustrates the reversible shape memory process, with the hydrogel lattice switching between a negative Poisson's ratio structure and a positive Poisson's ratio structure in saturated $CaCl_2$ and NaOH at equilibrium. Similarly, Figure 4b shows the hydrogel transforming between a negative Poisson's ratio structure and a zero Poisson's ratio structure. This shape memory process follows the multi-shape memory hydrogel mechanism involving chitosan network formation, as discussed in Section 3.3, which demonstrated nearly 100% shape fixity and recovery during the first cycle. However, as described in Section 3.2, the structural transformation may become slightly limited after multiple rounds, as indicated by the reduced shape fixity observed (Figure 2d). This reduction in shape fixity is typical of shape memory hydrogels due to the limited cyclic stability of the hydrogel's temporary crosslinks, which leads to some deformation over repeated cycles[52]. Despite this, we observed that the temporary shapes of the hydrogel lattice remained well-preserved with minimal degradation after three cycles of shape transformation (Figure S4 of the Supporting Information). Furthermore, the hydrogel lattice can be readily reconfigured by fixing it into a new temporary shape after returning to its original configuration, owing to its high reversibility. This reconfigurability enhances the hydrogel's versatility, making it suitable for dynamic and adaptable applications.

Furthermore, a multi-stage shape memory process is shown as illustrated in Figure 4c. In this process, a printed negative Poisson's ratio structure is first fixed into its primary shape as a zero Poisson's ratio structure, referred to as *Temporary Shape A*, in 5 M $CaCl_2$. It is then further fixed into a positive Poisson's ratio structure, referred to as *Temporary Shape B*, in saturated $CaCl_2$, and can revert to its original shape when placed in DI water. This demonstrates the hydrogel's shape adaptability across various $CaCl_2$ concentrations, allowing for different temporary shapes. At 5 M $CaCl_2$, a second chitosan network is partially formed, corresponding to *Temporary Shape A*, while increasing the $CaCl_2$ concentration to saturation enhances the chitosan network formation, achieving *Temporary Shape B*. These findings confirm that the reversible shape memory hydrogel can be employed to create complex and functional structures, such as lattice configurations, which are challenging to achieve with more rigid materials such as polymers or metals. This adaptability and versatility allow the lattice structure to mechanically respond to various environmental stimuli and to be reconfigured into new shapes as required.

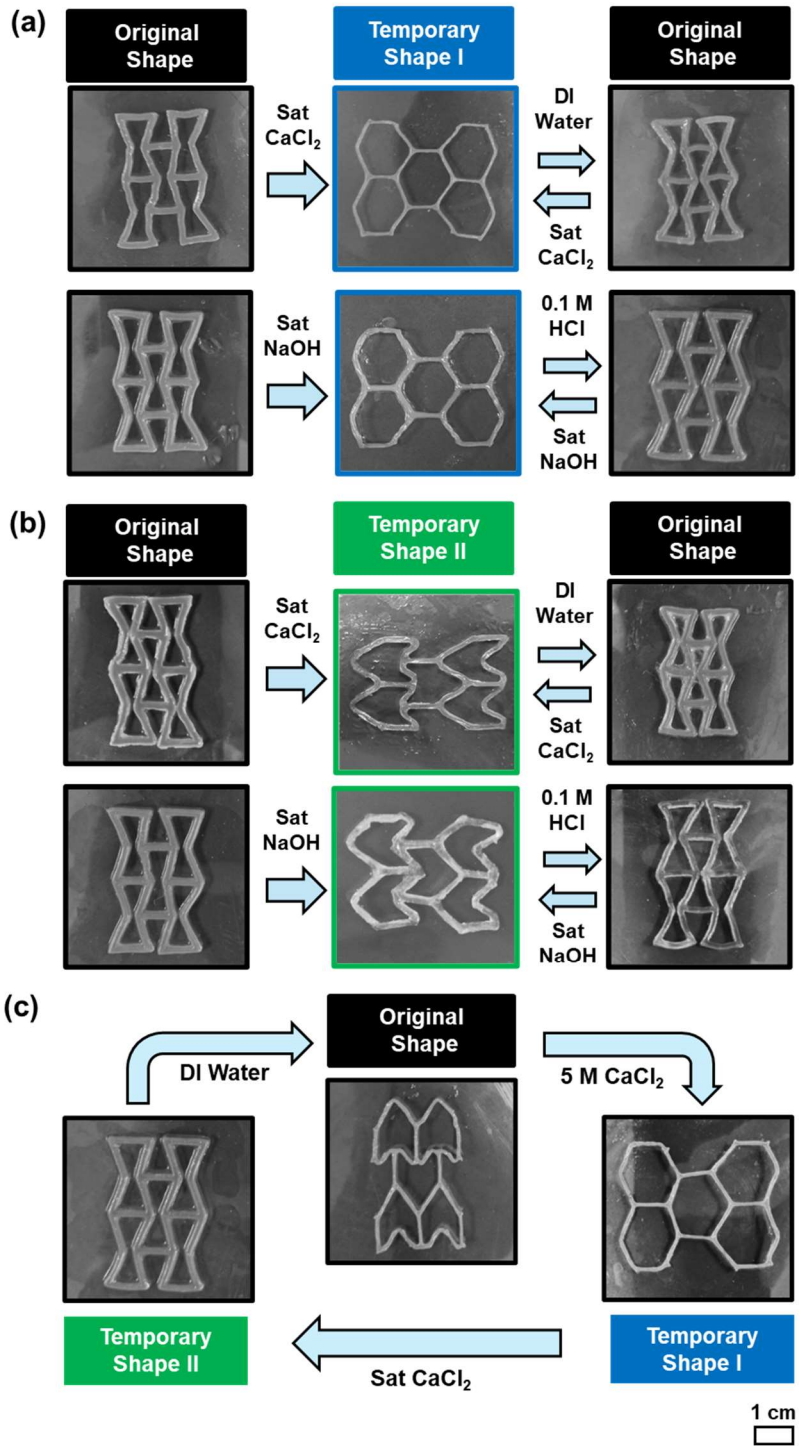

Figure 4. Multi-shape memory behavior of polyacrylic acid/chitosan hydrogels demonstrating tunable auxeticity in various solutions at equilibrium. Reversible shape memory process with the hydrogels transforming (a) between negative and positive Poisson's ratio structures, and (b) between negative and zero Poisson's ratio structures, both in saturated $CaCl_2$ and NaOH solutions. The recovery time is set to 25 minutes. (c) Multi-stage shape

memory process with the hydrogels transitioning from negative to zero and then to positive Poisson's ratio structures in solutions with varying $CaCl_2$ concentrations. Each image includes a 1 cm scale bar located at the bottom right.

Each lattice structure is engineered to respond mechanically in unique ways, exhibiting various auxetic properties characterized by negative, zero, and positive Poisson's ratios. This characteristic of mechanical metamaterials arises from the structural design rather than the intrinsic properties of the material. Consequently, alterations in the hydrogel shape of the lattice structure result in corresponding changes to the auxetic behavior. As illustrated in Figure 5, the *Original Shape* of the lattice structure displayed a negative Poisson's ratio, reaching a minimum value of -1.2 at 80% tensile strain. Upon being shape-fixed in saturated $CaCl_2$ until equilibrium, it transformed into *Temporary Shape I*, resulting in a Poisson's ratio that transitions to a positive value of 2.0 at the same strain of 80%. In contrast, *Temporary Shape II*, formed in saturated NaOH, exhibits a Poisson's ratio approaching zero at the same strain. These findings demonstrate the hydrogel lattice structure's ability to transition among three distinct shapes, each showcasing different auxetic properties—ranging from negative to zero and positive—while facilitating reversible mechanical responses.

Figure 5a (with the inserted rectangle and red dashed line) shows that the lattice structure in its *Original Shape*, which has a negative Poisson's ratio, expands laterally when stretched longitudinally. In contrast, when the lattice structure is transformed into *Temporary Shape I* in $CaCl_2$, it shrinks laterally instead of expanding when stretched longitudinally, due to the positive Poisson's ratio of the structure. Temporary Shape II in NaOH, which exhibits a zero Poisson's ratio, shows negligible lateral change when stretched. This further confirmed

the consistency of the measured Poisson's ratio and the structural design's ability to induce different mechanical metamaterial responses.

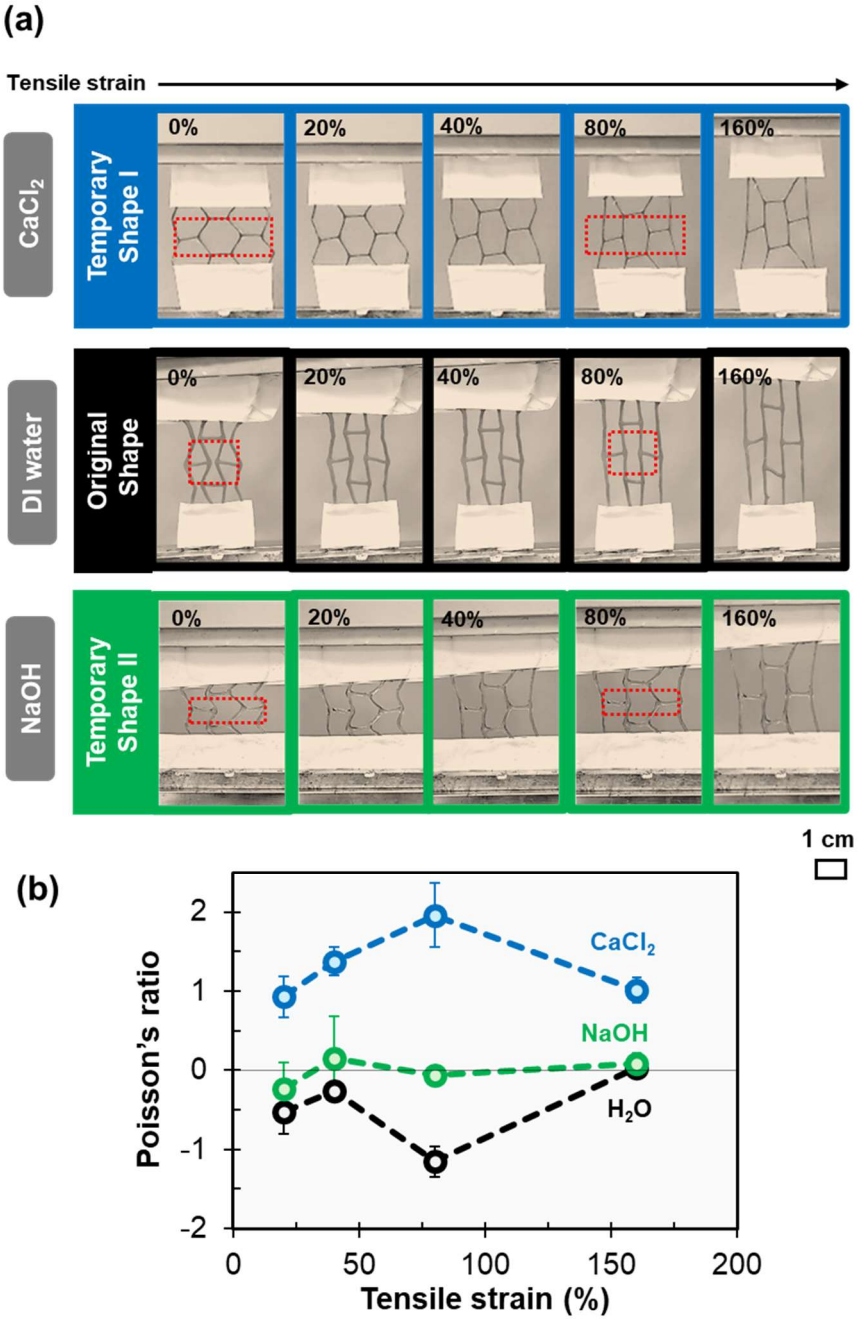

Figure 5. Experimental auxetic behavior of polyacrylic acid/chitosan hydrogels in various solutions at equilibrium. (a) Auxetic response of hydrogel structures in DI water, saturated $CaCl_2$, and NaOH under varying tensile strains. All images include a 1 cm scale bar. (b)

Measured correspond Poisson's ratio of hydrogel structures in DI water, $CaCl_2$, and NaOH at different tensile strains.

3.5 Finite Element Analysis of Hydrogel Lattice Structures

Finite Element Analysis (FEA) was conducted to confirm the auxetic behavior of the lattice structures, as shown in Figure 6 and to compare it with the experimental results in Figure 5. The simulation employed different material parameters based on the measured properties in DI water, saturated $CaCl_2$, and saturated NaOH (Table S1). The bottom side of each lattice structure was fixed while the top side was stretched longitudinally up to 160% strain to replicate the conditions of the mechanical test in Figure 5. The color gradient indicates the relative displacement from the original position along the X and Y directions.

For the *Original Shape* in DI water, as shown in Figure 6a, each unit cell and the overall structure expand laterally when stretched longitudinally, particularly beyond 80% strain, which is further illustrated in Figure 6b. This result aligns with and confirms the experimental observations. In the case of *Temporary Shape I* in saturated $CaCl_2$, the structure exhibits lateral shrinkage when stretched longitudinally beyond 80% strain, while *Temporary Shape II* in saturated NaOH demonstrates minimal lateral change when stretched to its maximum setting. The Poisson's ratios measured in each case, as presented in Figure 6b, align with the trend observed in the experimental results, though the absolute values differ due to the limitations of the FEA simulation[53, 54]. The shape deformation observed in the FEA simulations appeared to be less than that in the experimental results, likely because simulations are idealized and may not account for all factors influencing deformation, such as material heterogeneity or non-uniform stress distribution. Nonetheless, this FEA simulation validates the auxetic behavior of each lattice structure from a design perspective, supporting the experimental findings.

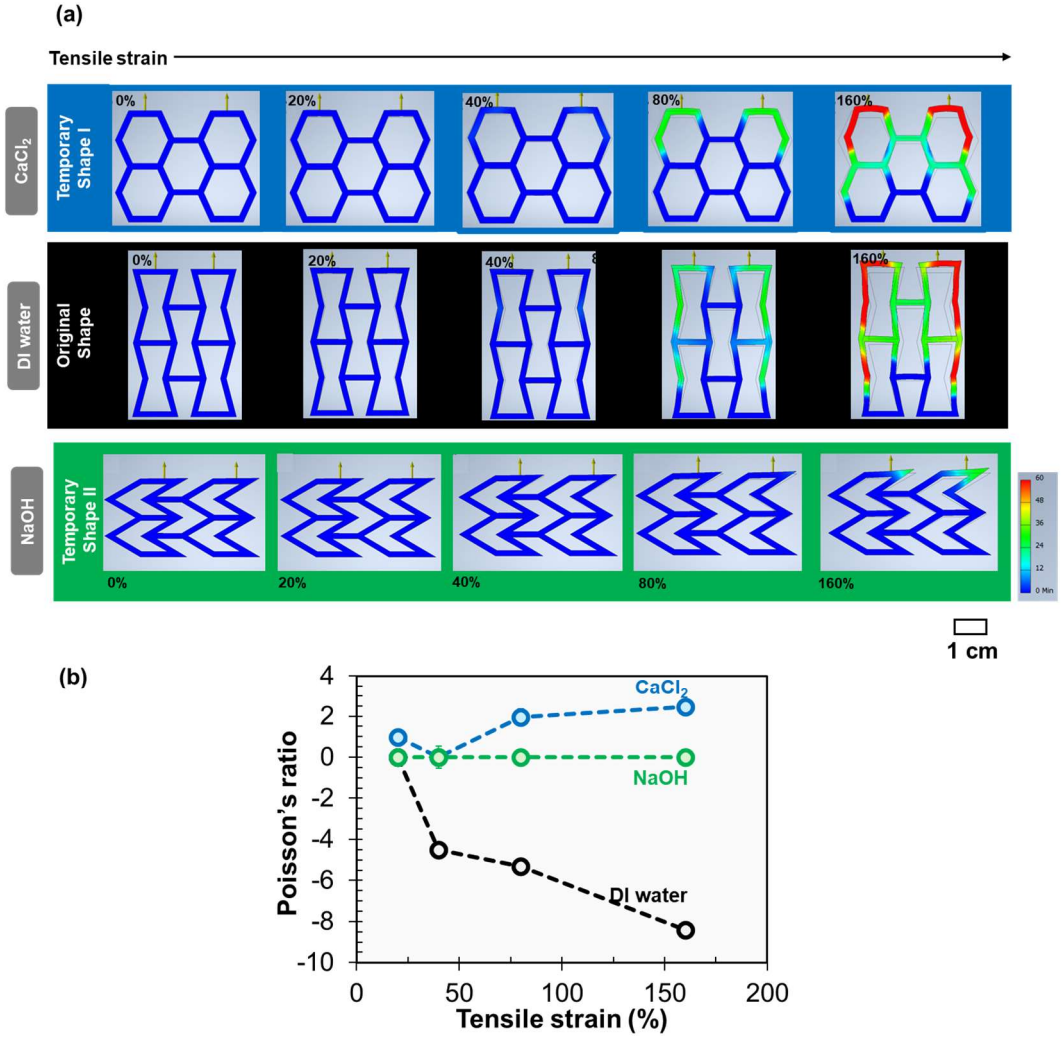

Figure 6. Finite Element Analysis (FEA)-based auxetic behavior of polyacrylic acid/chitosan hydrogels in various solutions. (a) Auxetic response of hydrogel structures in DI water, saturated $CaCl_2$, and NaOH under different tensile strains. All images include a 1 cm scale bar. The color scale bar indicates the relative displacement upon stretching the samples, measured in mm. (b) Measured Poisson's ratio of hydrogel structures in DI water, saturated $CaCl_2$, and NaOH at different tensile strains.

3.6 Potential Applications of Hydrogel-Based Metamaterials in Biomedical Stents

Due to their transformable auxeticity in response to external stimuli, the developed hydrogel lattices can be used to fabricate various smart and adaptive devices, particularly for biomedical applications such as soft robotics, sensors, and actuators. Hydrogels are generally highly biocompatible compared to other materials, with polyacrylic acid-chitosan hydrogels being particularly biocompatible and suitable for long-term use due to the inherent biocompatibility of their individual components (chitosan and polyacrylic acid)[55-58]. However, their final biocompatibility should be verified through more specific tests in the intended biological environment. Furthermore, the responsive properties of these hydrogels can be tailored to suit specific environmental conditions in applications, such as temperature or light sensitivity. This section presents a potential application of a hydrogel lattice with transformable auxeticity as a multi-mode biomedical stent (Figure 7). This stent is characterized by its ability to adapt its expansion mode in response to different external stimuli. The tunable auxeticity enables the stent to exhibit different modes of expansion depending on the soaked solution during stretching: (1) expandable mode in DI water, (2) shrinkable mode in saturated $CaCl_2$, and (3) non-expandable mode in saturated NaOH, as depicted in Figure 1. For practical applications, the critical concentration range for shape transformation activation and deactivation can be carefully considered and tuned. For example, a stent can be designed to activate into a shrinkable mode when the $CaCl_2$ concentration exceeds a threshold and revert to an expandable mode when the concentration decreases. Such salt-responsive materials show potential for human body applications, such as wound healing and tissue engineering[59-61]. The stent, characterized by a negative Poisson's ratio structure, is fabricated through 3D printing and subsequently shape-fixed within a 3D mold, resulting in either a positive Poisson's ratio structure in $CaCl_2$ or a zero Poisson's ratio structure in saturated NaOH solution (Figure S5 of the Supporting Information). The mechanical response of the fabricated stent is assessed by

evaluating the diameter change ratio (DCR) during stretching, using both experimental methods and FEA simulations.

In its original state in DI water, the stent demonstrates a significant increase in DCR upon stretching, reaching peak values of 20% in experiments and 14% in simulations, indicative of its negative Poisson's ratio (expandable mode) (Figures 7b and 7c). Conversely, when shape-fixed in saturated $CaCl_2$ with a positive Poisson's ratio structure, the stent tends to shrink rather than expand during stretching, with peak DCR values of -9.4% in experiments and -5% in simulations (shrinkable mode). Notably, when the stent is subsequently soaked in DI water, it reversibly returns to its original shape, maintaining the expandable mode.

Further shape-fixing in saturated NaOH, corresponding to a zero Poisson's ratio structure, led to minimal changes in the stent's DCR (non-expandable mode). These findings correlate with the transitional nature of Poisson's ratio—negative, positive, and zero—within the lattice structure, as discussed in Sections 3.4 and 3.5, highlighting the potential for multi-mode stents with tunable expansion characteristics. This confirms the shape memory performance of the stent under different stimuli through the adaptive mechanical characteristics of the various lattice structures. The transformable and reconfigurable hydrogel-based mechanical metamaterials developed here demonstrate remarkable mechanical adaptability in response to various external stimuli, emphasizing their strong potential for advanced biomedical applications. This adaptability combines the unique shape memory, softness, responsiveness, and biocompatibility of hydrogels with the mechanical functionality and high customizability of metamaterials.

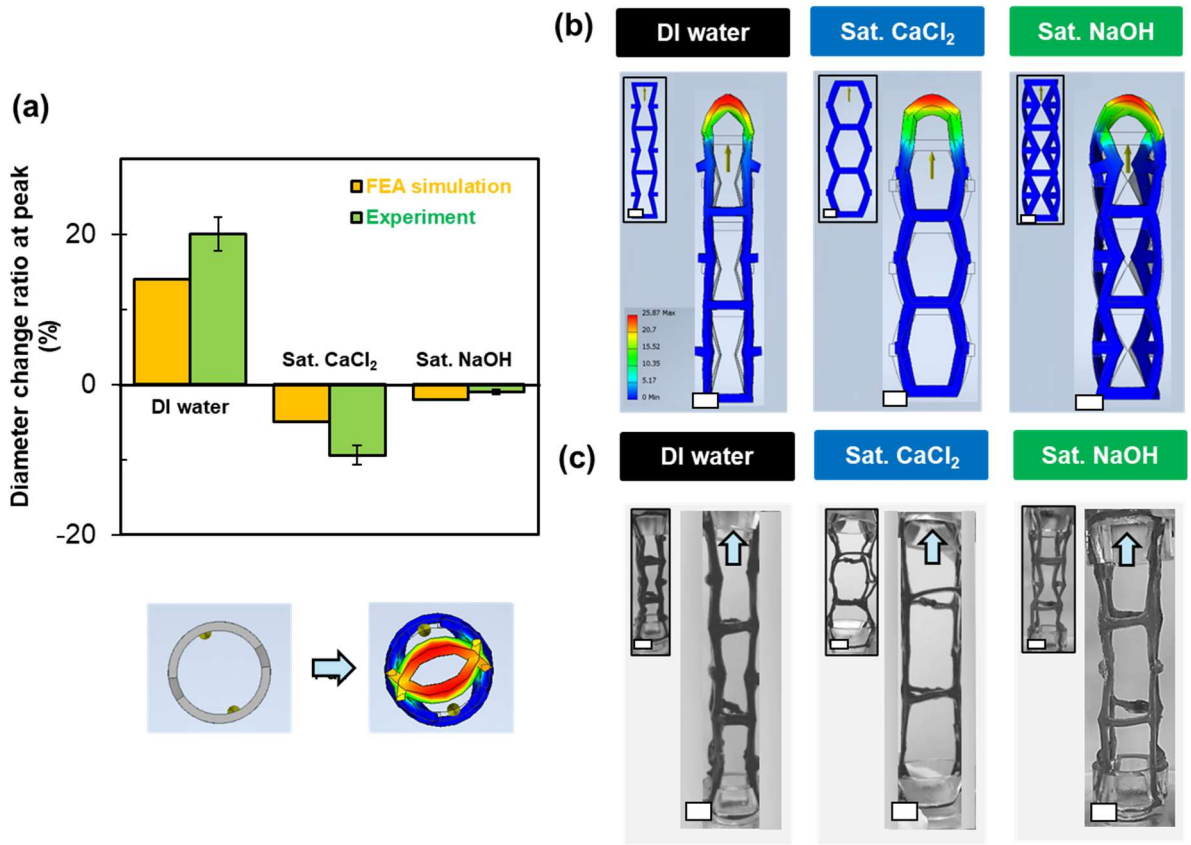

Figure 7. Applications of hydrogel-based metamaterials as biomedical stents. (a) Diameter change ratio (DCR) at peak for the hydrogel stent soaked in DI water, saturated $CaCl_2$, and saturated NaOH, measured through FEA simulation and experiments. The inset shows the diameter change after stretching, illustrated from the top view of the stent in the simulation (DI water). (b) and (c) Finite element analysis (FEA) simulations and experimental mechanical testing of the hydrogel stent soaked in DI water, saturated $CaCl_2$, and NaOH, conducted both before (top left) and after (right) stretching at peak DCR. The strain limit is up to 700%. The color scale bar represents the relative displacement upon stretching the samples, measured in mm.

4. Conclusions

Here, we developed hydrogel-based metamaterials with enhanced mechanical adaptability by integrating multi-shape-memory polyacrylic acid (PAA)-chitosan hydrogels into a lattice structure design. Leveraging the hydrogel's high fixity ratio, reversibility, and softness, the fabricated hydrogel-based metamaterials demonstrate unique mechanical responses, with transformable Poisson's ratios that shift from negative in deionized (DI) water to positive in saline solutions and to zero in alkaline solutions. This response is driven by structural adjustments in the soft hydrogels' shape memory process, which results from the formation and removal of secondary and tertiary chitosan networks within the PAA hydrogel. Its potential is further demonstrated through its application as a multi-mode biomedical stent, highlighting its practicality for real-world use. The stent can dynamically and reversibly transition between states—expandable, shrinkable, and non-expandable—each with distinct Poisson's ratios. This advancement highlights the potential of integrating metamaterial design with multi-shape-memory, soft, and responsive materials within a lattice structure framework to develop smart, versatile biomaterials for biomedical applications.

Acknowledgments

This work was financially supported by the A*STAR Career Development Fund (C233312015) and MTC Individual Research Grants (M23M6c0110). We extend our gratitude to Hannah Hui Ling Lim and Anna Marie Yong of IMRE for her invaluable laboratory support.

Supporting Information

The following Supporting Information is available for this article:

- Figure S1. 3D models of hydrogel lattice structures.

- Figure S2. Shape fixation protocol for hydrogel lattice structure.
- Figure S3. 3D models of hydrogel stents.
- Figure S4. Shape memory process of the hydrogel lattice after three cycles of shape transformation.
- Figure S5. Shape fixation protocol for hydrogel stent.
- Table S1. Material parameters of polyacrylic acid/chitosan hydrogel in DI water, saturated $CaCl_2$, and saturated NaOH for Finite Element Analysis (FEA) simulation.
- Table S2. Summary of the mechanical properties of the polyacrylic acid/chitosan hydrogel in DI water, saturated $CaCl_2$, and saturated NaOH.

Data Availability Statement

The data presented in this study are available on request from the corresponding author.

Conflict of Interest

The authors declare that they have no conflict of interest.

Contributions

S.P. conceived the idea, developed the outline, designed the experiments, and prepared the draft manuscript. R.L.J.T., Y.H.C., and S.P. prepared the samples and performed the experimental measurements. E.L.L.N., Y.T.C., and F.W. provided support for the experiments. R.L.J.T. conducted the FEA simulations. S.P., R.L.J.T., Y.H.C., and F.W. analyzed the data and contributed to writing the manuscript.

References

1. Jiao, P.; Mueller, J.; Raney, J. R.; Zheng, X.; Alavi, A. H., Mechanical Metamaterials and Beyond. *Nature Communications* **2023,** *14* (1), 6004.

2. Zadpoor, A. A., Mechanical Meta-Materials. *Materials Horizons* **2016,** *3* (5), 371.

3. Surjadi, J. U.; Gao, L.; Du, H.; Li, X.; Xiong, X.; Fang, N. X.; Lu, Y., Mechanical Metamaterials and Their Engineering Applications. *Advanced Engineering Materials* **2019,** *21* (3), 1800864.

4. Zhou, X.; Ren, L.; Song, Z.; Li, G.; Zhang, J.; Li, B.; Wu, Q.; Li, W.; Ren, L.; Liu, Q., Advances in 3D/4D Printing of Mechanical Metamaterials: From Manufacturing to Applications. *Composites Part B: Engineering* **2023,** *254*, 110585.

5. Gao, J.; Cao, X.; Xiao, M.; Yang, Z.; Zhou, X.; Li, Y.; Gao, L.; Yan, W.; Rabczuk, T.; Mai, Y.-W., Rational Designs of Mechanical Metamaterials: Formulations, Architectures, Tessellations and Prospects. *Materials Science and Engineering: R: Reports* **2023,** *156*, 100755.

6. Ren, X.; Shen, J.; Ghaedizadeh, A.; Tian, H.; Min Xie, Y., Experiments and Parametric Studies on 3D Metallic Auxetic Metamaterials with Tuneable Mechanical Properties. *Smart Materials and Structures* **2015,** *24* (9), 095016.

7. Deng, B.; Xu, R.; Zhao, K.; Lu, Y.; Ganguli, S.; Cheng, G. J., Composite Bending-Dominated Hollow Nanolattices: A Stiff, Cyclable Mechanical Metamaterial. *Materials Today* **2018,** *21* (5), 467.

8. Veerabagu, U.; Palza, H.; Quero, F., Review: Auxetic Polymer-Based Mechanical Metamaterials for Biomedical Applications. *ACS Biomaterials Science & Engineering* **2022,** *8* (7), 2798.

9. Cui, S.; Gong, B.; Ding, Q.; Sun, Y.; Ren, F.; Liu, X.; Yan, Q.; Yang, H.; Wang, X.; Song, B., Mechanical Metamaterials Foams with Tunable Negative Poisson's Ratio for Enhanced Energy Absorption and Damage Resistance. *Materials* **2018,** *11* (10), 1869.

10. Ma, L.-H.; Wang, S.-D.; Liu, J.; Gao, H.; Zhou, W., The Design and Investigation of Hydrogel-Based Metamaterials with Ultra Large Negative Hygroscopic Expansion Ratio. *International Journal of Smart and Nano Materials* **2022,** *13* (1), 114.

11. Yigci, D.; Ahmadpour, A.; Tasoglu, S., AI-Based Metamaterial Design for Wearables. *Advanced Sensor Research* **2024,** *3* (3), 2300109.

12. Jiang, S.; Liu, X.; Liu, J.; Ye, D.; Duan, Y.; Li, K.; Yin, Z.; Huang, Y., Flexible Metamaterial Electronics. *Advanced Materials* **2022,** *34* (52), 2200070.

13. Pruksawan, S.; Chee, H. L.; Wang, Z.; Luo, P.; Chong, Y. T.; Thitsartarn, W.; Wang, F., Toughened Hydrogels for 3D Printing of Soft Auxetic Structures. *Chemistry – An Asian Journal* **2022,** *17* (19), e202200677.

14. Tsegay, F.; Hisham, M.; Elsherif, M.; Schiffer, A.; Butt, H., 3D Printing of pH Indicator Auxetic Hydrogel Skin Wound Dressing. *Molecules* **2023,** *28* (3), 1339.

15. Zhang, W.; Soman, P.; Meggs, K.; Qu, X.; Chen, S., Tuning the Poisson's Ratio of Biomaterials for Investigating Cellular Response. *Advanced Functional Materials* **2013,** *23* (25), 3226.

16. Liu, X.; Gao, M.; Chen, J.; Guo, S.; Zhu, W.; Bai, L.; Zhai, W.; Du, H.; Wu, H.; Yan, C.; Shi, Y.; Gu, J.; Qi, H. J.; Zhou, K., Recent Advances in Stimuli-Responsive Shape-Morphing Hydrogels. *Advanced Functional Materials* **2022,** *32* (39), 2203323.

17. Lavrador, P.; Esteves, M. R.; Gaspar, V. M.; Mano, J. F., Stimuli-Responsive Nanocomposite Hydrogels for Biomedical Applications. *Advanced Functional Materials* **2021,** *31* (8), 2005941.

18. Jeon, S.-J.; Hauser, A. W.; Hayward, R. C., Shape-Morphing Materials from Stimuli-Responsive Hydrogel Hybrids. *Accounts of Chemical Research* **2017,** *50* (2), 161.

19. Pruksawan, S.; Chua, Z. A.; Chong, Y. T.; Loh, T. J. E.; Ng, E. L. L.; Wang, F., Smart Hydrogel-Based Mechanical Metamaterials: A Review. *ACS Applied Polymer Materials* **2024,** *6* (20), 12362.

20. Zhang, M.; Pal, A.; Zheng, Z.; Gardi, G.; Yildiz, E.; Sitti, M., Hydrogel Muscles Powering Reconfigurable Micro-Metastructures with Wide-Spectrum Programmability. *Nature Materials* **2023,** *22* (10), 1243.

21. Guo, H.; Cheng, J.; Yang, K.; Demella, K.; Li, T.; Raghavan, S. R.; Nie, Z., Programming the Shape Transformation of a Composite Hydrogel Sheet Via Erasable and Rewritable Nanoparticle Patterns. *ACS Applied Materials & Interfaces* **2019,** *11* (45), 42654.

22. Chen, Z.; Li, Y.; Li, Q. M., Hydrogel-Driven Origami Metamaterials for Tunable Swelling Behavior. *Materials & Design* **2021,** *207*, 109819.

23. Zhao, H.; Pan, S.; Natalia, A.; Wu, X.; Ong, C.-A. J.; Teo, M. C. C.; So, J. B. Y.; Shao, H., A Hydrogel-Based Mechanical Metamaterial for the Interferometric Profiling of Extracellular Vesicles in Patient Samples. *Nature Biomedical Engineering* **2023,** *7* (2), 135.

24. Hu, Y.; Guo, Z.; Ragonese, A.; Zhu, T.; Khuje, S.; Li, C.; Grossman, J. C.; Zhou, C.; Nouh, M.; Ren, S., A 3D-Printed Molecular Ferroelectric Metamaterial. *Proceedings of the National Academy of Sciences* **2020,** *117* (44), 27204.

25. Chansoria, P.; Blackwell, J.; Etter, E. L.; Bonacquisti, E. E.; Jasiewicz, N.; Neal, T.; Kamal, S. A.; Hoque, J.; Varghese, S.; Egan, T.; Nguyen, J., Rationally Designed Anisotropic and Auxetic Hydrogel Patches for Adaptation to Dynamic Organs. *Advanced Functional Materials* **2022,** *32* (43), 2207590.

26. Qiu, Y.; Ye, H.; Zhang, S.; Zhang, H.; Zheng, Y., Hydrogel-Based Network Metamaterials with Biological Tissue-Like Poisson's Ratio Behavior and Stress Response. *ACS Applied Materials & Interfaces* **2024,** *16* (45), 62371.

27. Yang, H.; D'Ambrosio, N.; Liu, P.; Pasini, D.; Ma, L., Shape Memory Mechanical Metamaterials. *Materials Today* **2023,** *66*, 36.

28. Gu, H.; Dong, X.; Zhang, Q.; Chi, D.; Zhang, Y.; Cheng, Z.; Lv, T.; Xie, Z.; Xu, Y.; Zhang, D.; Liu, Y., Intelligent Reversible Reconfigurable Metamaterials Based on a Two-Way Shape Memory Polymer. *ACS Applied Materials & Interfaces* **2024,** *16* (40), 54627.

29. Pirhaji, A.; Jebellat, E.; Roudbarian, N.; Mohammadi, K.; Movahhedy, M. R.; Asle Zaeem, M., Large Deformation of Shape-Memory Polymer-Based Lattice Metamaterials. *International Journal of Mechanical Sciences* **2022,** *232*, 107593.

30. Zhao, W.; Li, N.; Liu, X.; Liu, L.; Yue, C.; Zeng, C.; Liu, Y.; Leng, J., 4D Printed Shape Memory Metamaterials with Sensing Capability Derived from the Origami Concept. *Nano Energy* **2023,** *115*, 108697.

31. Wu, Y.; Han, Y.; Wei, Z.; Xie, Y.; Yin, J.; Qian, J., 4D Printing of Chiral Mechanical Metamaterials with Modular Programmability Using Shape Memory Polymer. *Advanced Functional Materials* **2023,** *33* (52), 2306442.

32. Pruksawan, S.; Lim, J. W. R.; Lee, Y. L.; Lin, Z.; Chee, H. L.; Chong, Y. T.; Chi, H.; Wang, F., Enhancing Hydrogel Toughness by Uniform Cross-Linking Using Modified Polyhedral Oligomeric Silsesquioxane. *Communications Materials* **2023,** *4* (1), 75.

33. Xiao, H.; Ma, C.; Le, X.; Wang, L.; Lu, W.; Theato, P.; Hu, T.; Zhang, J.; Chen, T., A Multiple Shape Memory Hydrogel Induced by Reversible Physical Interactions at Ambient Condition. *Polymers* **2017,** *9* (4), 138.

34. Wang, X.-H.; Song, F.; Xue, J.; Qian, D.; Wang, X.-L.; Wang, Y.-Z., Mechanically Strong and Tough Hydrogels with Excellent Anti-Fatigue, Self-Healing and Reprocessing Performance Enabled by Dynamic Metal-Coordination Chemistry. *Polymer* **2018,** *153*, 637.

35. Li, X.; Xu, S.; Wang, Y.; Hu, Z.-Y.; Wang, R., A High Strength Hydrogel with Quadruple-Shape Memory under the Ambient Condition. *Colloid and Polymer Science* **2019,** *297* (4), 503.

36. Lu, Z.; Zou, L.; Zhou, X.; Huang, D.; Zhang, Y., High Strength Chitosan Hydrogels Prepared from NaOH/Urea Aqueous Solutions: The Role of Thermal Gelling. *Carbohydrate Polymers* **2022,** *297*, 120054.

37. Zheng, B.-B.; Liu, F.-M.; Hu, L.-L.; Fu, M.-H.; Chen, Y., An Auxetic Honeycomb Structure with Series-Connected Parallograms. *International Journal of Mechanical Sciences* **2019,** *161-162*, 105073.

38. Chang, Y.; Hu, H., 3D Fabrics with Negative Poisson's Ratio: A Review. *Applied Composite Materials* **2022,** *29* (1), 95.

39. Cho, H.; Seo, D.; Kim, D.-N., Mechanics of Auxetic Materials. In *Handbook of Mechanics of Materials*, Schmauder, S.; Chen, C.-S.; Chawla, K. K.; Chawla, N.; Chen, W.; Kagawa, Y., Eds. Springer: Singapore, 2019; pp 733.

40. Sahariah, B. J.; Baishya, M. J.; Namdeo, A.; Khanikar, P., A Novel Strategy to Design Lattice Structures with Zero Poisson's Ratio. *Engineering Structures* **2023,** *288*, 116214.

41. Ali, M. N.; Busfield, J. J. C.; Rehman, I. U., Auxetic Oesophageal Stents: Structure and Mechanical Properties. *Journal of Materials Science: Materials in Medicine* **2014,** *25* (2), 527.

42. Ali, M. N.; Rehman, I. U., An Auxetic Structure Configured as Oesophageal Stent with Potential to be Used for Palliative Treatment of Oesophageal Cancer; Development and in Vitro Mechanical Analysis. *Journal of Materials Science: Materials in Medicine* **2011,** *22* (11), 2573.

43. Wang, W.; Xue, C.; Mao, X., Chitosan: Structural Modification, Biological Activity and Application. *International Journal of Biological Macromolecules* **2020,** *164*, 4532.

44. Wu, X. L.; Huang, W. M.; Lu, H. B.; Wang, C. C.; Cui, H. P., Characterization of Polymeric Shape Memory Materials. *Journal of Polymer Engineering* **2017,** *37* (1), 1.

45. Mo, K.; Zhang, T.; Yan, W.; Chang, C., Tunicate Cellulose Nanocrystal Reinforced Polyacrylamide Hydrogels with Tunable Mechanical Performance. *Cellulose* **2018,** *25* (11), 6561.

46. Yang, J.; Deng, L.-H.; Han, C.-R.; Duan, J.-F.; Ma, M.-G.; Zhang, X.-M.; Xu, F.; Sun, R.-C., Synthetic and Viscoelastic Behaviors of Silica Nanoparticle Reinforced Poly(Acrylamide) Core–Shell Nanocomposite Hydrogels. *Soft Matter* **2013,** *9* (4), 1220.

47. Sujan, M. I.; Sarkar, S. D.; Sultana, S.; Bushra, L.; Tareq, R.; Roy, C. K.; Azam, M. S., Bi-Functional Silica Nanoparticles for Simultaneous Enhancement of Mechanical Strength and Swelling Capacity of Hydrogels. *RSC Advances* **2020,** *10* (11), 6213.

48. Yang, C. H.; Wang, M. X.; Haider, H.; Yang, J. H.; Sun, J.-Y.; Chen, Y. M.; Zhou, J.; Suo, Z., Strengthening Alginate/Polyacrylamide Hydrogels Using Various Multivalent Cations. *ACS Applied Materials & Interfaces* **2013,** *5* (21), 10418.

49. Li, S.-N.; Li, B.; Gong, L.-X.; Yu, Z.-R.; Feng, Y.; Jia, D.; Zhou, Y.; Tang, L.-C., Enhanced Mechanical Properties of Polyacrylamide/Chitosan Hydrogels by Tuning the Molecular Structure of Hyperbranched Polysiloxane. *Materials & Design* **2019,** *162*, 162.

50. Chen, X.; Cai, L.; Wen, J., Extreme Mechanical Metamaterials with Independently Adjustable Elastic Modulus and Mass Density. *Applied Physics Express* **2022,** *15* (4), 047001.

51. Zhang, R.; Chang, S. J.; Jing, Y.; Wang, L.; Chen, C.-J.; Liu, J.-T., Application of Chitosan with Different Molecular Weights in Cartilage Tissue Engineering. *Carbohydrate Polymers* **2023,** *314*, 120890.

52. Lee, A. Y.; An, J.; Chua, C. K., Two-Way 4D Printing: A Review on the Reversibility of 3D-Printed Shape Memory Materials. *Engineering* **2017,** *3* (5), 663.

53. Kumar, V.; Mistri, A.; Jain, V.; Ghosh, M., Computational Engineering for 3D Bioprinting. In *3D Bioprinting from Lab to Industry*, 2024; pp 301.

54. Caccavo, D.; Cascone, S.; Lamberti, G.; Barba, A. A., Hydrogels: Experimental Characterization and Mathematical Modelling of Their Mechanical and Diffusive Behaviour. *Chemical Society Reviews* **2018,** *47* (7), 2357.

55. Mohamed, R. R.; Elella, M. H. A.; Sabaa, M. W., Cytotoxicity and Metal Ions Removal Using Antibacterial Biodegradable Hydrogels Based on N-Quaternized Chitosan/Poly(Acrylic Acid). *International Journal of Biological Macromolecules* **2017,** *98*, 302.

56. Pal, K.; Kumar, S.; Yadav, P.; Jaiswal, S.; Kumar, R.; Acharya, A., Chitosan-Based Self-Healing Hydrogel Mediated by Poly(Acrylic-Methacrylic Acid) Exhibiting High Biocompatibility and Anti-Tumor Activity. *Journal of Applied Polymer Science* **2024,** *141* (46), e56231.

57. Peniche, C.; Argüelles-Monal, W.; Peniche, H.; Acosta, N., Chitosan: An Attractive Biocompatible Polymer for Microencapsulation. *Macromolecular Bioscience* **2003,** *3* (10), 511.

58. Wang, Y.; Wang, J.; Yuan, Z.; Han, H.; Li, T.; Li, L.; Guo, X., Chitosan Cross-Linked Poly(Acrylic Acid) Hydrogels: Drug Release Control and Mechanism. *Colloids and Surfaces B: Biointerfaces* **2017,** *152*, 252.

59. Yuan, J.; Zhang, D.; He, X.; Ni, Y.; Che, L.; Wu, J.; Wu, B.; Wang, Y.; Wang, S.; Sha, D.; Zheng, S. Y.; Yang, J., Cationic Peptide-Based Salt-Responsive Antibacterial Hydrogel Dressings for Wound Healing. *International Journal of Biological Macromolecules* **2021,** *190*, 754.

60. Fang, Y.; Huang, S.; Gong, X.; King, J. A.; Wang, Y.; Zhang, J.; Yang, X.; Wang, Q.; Zhang, Y.; Zhai, G.; Ye, L., Salt Sensitive Purely Zwitterionic Physical Hydrogel for Prevention of Postoperative Tissue Adhesion. *Acta Biomaterialia* **2023,** *158*, 239.

61. Sakthivel, M.; Franklin, D. S.; Sudarsan, S.; Chitra, G.; Sridharan, T. B.; Guhanathan, S., Investigation on pH/Salt-Responsive Multifunctional Itaconic Acid Based Polymeric Biocompatible, Antimicrobial and Biodegradable Hydrogels. *Reactive and Functional Polymers* **2018,** *122*, 9.

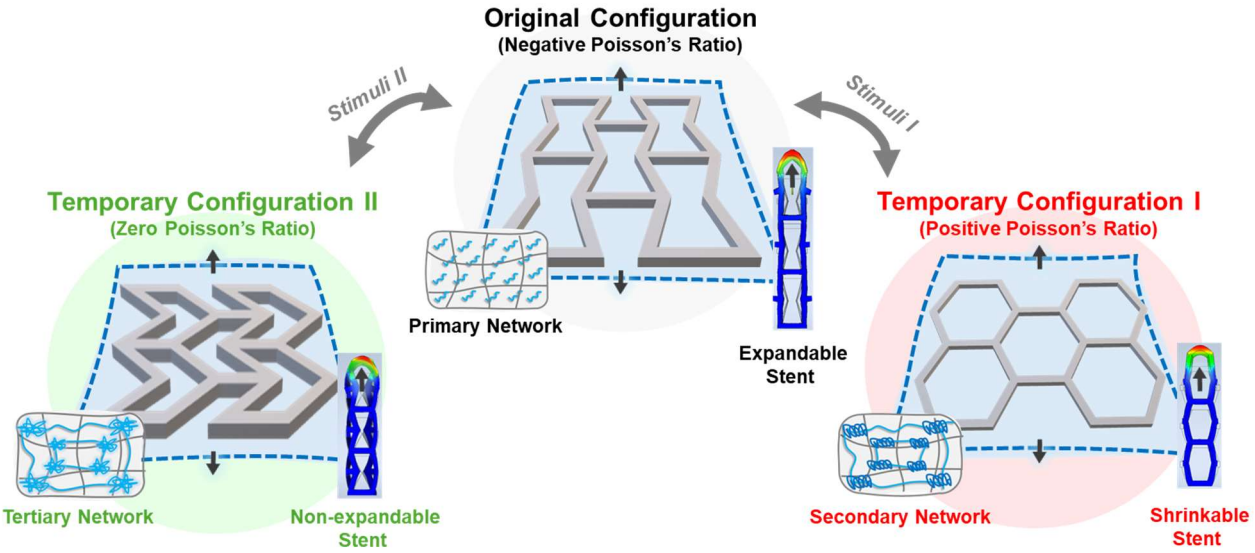

For Table of Contents Only